Localization of Ischemic Myocardial Segments from 12-Lead ECG Using the Spatial ECG

Vito Starc[1]

[1]University of Ljubljana, Faculty of Medicine, Ljubljana, Slovenia

Abstract

We investigated the potential clinical utility of our application based on inverse problem solving and providing the equivalent dipole trajectories (EDT) from 12-lead ECGs. EDTs represent the movement of the averaged current source through the heart during the heart cycle. We hypothesized that during acute myocardial ischemia, the ST segment EDTs orient and extend towards the myocardial segment supplied by the affected coronary artery, revealing the location of ischemia, which might aid its detection.

We extracted 382 signal specimens of ECG signals from 103 patients within the STAFF III database who underwent elective coronary artery occlusion. We related the EDT data to the modeled heart wall segments.

The localization of the corresponding myocardial segments was sound in the LAD and LCX arteries (in 92% of 145 and 96% of 72 specimens, respectively). It was deficient in the RCA artery (in 45% of 146 specimens), primarily due to the region overlap in segment No. 8.

1. Introduction

Several analytical methods have recently emerged to detect the location changes of the heart's current sources in different cardiac pathologies from the 12-lead ECG. These included the derivation of *CineECG* [1] or the assessment of moving equivalent dipoles (ED) and their trajectory (EDT) representing the movement of the averaged current source during the heart cycle [2, 3]. By relating measured ECG data to cardiac anatomy, these non-invasive methods introduce a novel scientific area, the spatial ECG. However, there were uncertainties in determining the exact spatial position of the EDT due to electrode mispositioning and anatomical model selection, calling for the necessity of medical imaging data. As the ECG recordings usually lack imaging data, we wondered whether determining EDs from 12-lead ECG could provide applicable results when missing these data.

In one of our previous studies using a spherically bounded volume conductor model, we found that the location and orientation of the ST segment's EDs change characteristically during the occlusion of different coronary arteries [2]. Here, we hypothesize that during acute myocardial ischemia, the EDTs at the end of the QRS interval and ST segment are orienting towards the myocardial segment supplied by the affected coronary artery, revealing the location of ischemia, which might aid its detection.

To test our hypothesis, we used the STAFF III database with patients who underwent elective balloon angioplasty with coronary artery occlusion [4].

2. Methods

To determine EDTs from the 12-lead ECG, we solved the inverse problem utilizing our upgraded boundary element model (BEM) method with an adaptable human torso model [5]. The BEM provided the forward model relating the ED properties and location to the surface potentials. To assess dipolar properties and locations, we varied EDTs to minimize the difference between the measured and calculated potential.

We applied two optimization steps. In the first, the trajectory was constructed using its reference position and speed propagation parameters, $\mathbf{r}_{ref}$ and $\mathbf{v}_{ref}$, respectively, which were varied to provide an optimal trajectory. We utilized eight differently shaped torsos, among which we selected the trajectory with the most minor error. That trajectory served as an initial approximation in the second optimization, in which we varied all dipolar locations $\mathbf{r}_k$ to minimize the error. We further optimized the electrode positioning and torso geometry to overcome deficiencies in imaging data.

2.1. Construction of a tailored torso model

The torso framework consisted of 24 vertically aligned rounded isosceles trapezoids with circles inscribed at the trapezoid corners. By dividing each trapezoid into 48 sectors, the outer torso surface provided 1152 discretized surfaces. The torso shape could be modified using the tailor's measures, such as height, waist width, and depth. We created eight torsos of different shapes and equal

volume by combining the torso measures (tall – short, wide - narrow, and thin – thick) differing by 15%.

2.2. Calculation of surface potentials

Using BEM, the central points of the torso's discretized surfaces at positions $\mathbf{r}_i$, i=1 to N, were utilized to determine surface potentials $\boldsymbol{\varphi}_i$ relating the distribution $\boldsymbol{\varphi}$ to the inverted matrix $\mathbf{A}^{-1}$ [6],

$$\boldsymbol{\varphi} = \mathbf{A}^{-1}\,\mathbf{g}. \qquad (1)$$

The matrix **A** depends only on the properties of the volume conductor. The vector **g** represents the potentials $\varphi_{\infty,ik}$ at $\mathbf{r}_i$ generated by dipole vector $\mathbf{D}_k$ (the current source) at position $\mathbf{r}_k$ in an infinite medium, $\varphi_{\infty,ik} = \boldsymbol{\rho}_{ik}\cdot\mathbf{D}_k$. Here, vector $\boldsymbol{\rho}_{ik}$ depends only on coordinates i and k. After separating the dipolar properties from those of the volume conductor in (1), we obtain

$$\varphi_{ik} = \mathbf{L}_{ik}\cdot\mathbf{D}_k, \qquad (2)$$

$\mathbf{L}_{ik} = \mathbf{A}^{-1}\boldsymbol{\rho}_{ik}$ is location $\mathbf{r}_k$ characteristic Burger's lead vector modified by $\mathbf{A}^{-1}$.

Eq. (2) represents an overdetermined system of Ni=9 equations, $\varphi_{ik} = L_{ikx}\cdot D_x + L_{iky}\cdot D_y + L_{iky}\cdot D_y$ in Cartesian coordinates. Solving it for D_x, D_y, and D_z utilizing a measured potential set V_i and a dipole at arbitrary location $\mathbf{r}_k$, the system provides the best $\mathbf{D}_k$ (not necessarily the optimal) and its orientation $\mathbf{c}_k$.

2.3. The ED trajectory propagation speed

A plausible hypothesis is that EDs are moving with the propagation speed v_{ED} in the direction of $\mathbf{c}_k$ from the location r_k to r_{k+1},

$$\overrightarrow{\boldsymbol{r}_{k\pm1}} = \overrightarrow{\boldsymbol{r}_k} \pm v_{ED}(t_k)\overrightarrow{\boldsymbol{c}_k}, \qquad (3)$$

where the sign ± represents the conduction to or from the reference point. We assumed that v_{ED} is steady in depolarization, $v_{ED}=v_{QRS}$, whereas in repolarization after the QRS end at time t_{QRSe}, it decays exponentially with a time constant tau approaching a steady value v_T at the T wave end,

$$v_{ED}(k) = \left(v_{QRS} - v_T\right)\cdot e^{-(t_k - t_{QRSe})/tau} \qquad (4)$$

The ED trajectory was constructed from the reference location, $\mathbf{r}_{ref} = (x, y, z)_{ref}$, starting at the peak QRS amplitude and spreading in both directions to reach the initial QRS and T wave end points using the formula.

2.4. Optimization of the EDT's localization

To find a dipolar trajectory (dipoles $\mathbf{D}_k$ with locations $\mathbf{r}_k$) that best describes measured signals $\mathbf{V}_{ik}$, denoting signal samples with index k, we applied an optimization method with the objective function $\psi(\mathbf{r}_k)$ minimizing the error $Err = 1 - R_{cc}$ between the model predicted and measured potentials with N_l signals each with N_k samples,

$$\psi(\boldsymbol{r}_k) = \mathrm{Err} + \sum_k^{N_k}\left(\sum_i^{N_l}\|R\|\right).$$

Here, R_{cc} is the cross-correlation coefficient,

$$Rcc = \frac{\sum_i^{N_i}\sum_k^{N_k}\varphi_{ik}V_{ik}}{\sqrt{\sum_i^{N_i}\sum_k^{N_k}\varphi_{ik}^2\cdot\sum_i^{N_i}\sum_k^{N_k}V_{ik}^2}}. \qquad (5)$$

Furthermore, R represents some positive valued regularizing function [7], such as the trajectory curvature, deviation from the measured electrode position, local conductivities, or the Wilson central terminal.

We applied two optimization steps. In the first step, the trajectory was modeled utilizing the reference position parameters, $\mathbf{r}_{ref}$, and calculating the propagation speed, v_{ED}, using (3) and (4). Applying the Nelder-Mead algorithm [8], we varied the parameters v_{ED} and v_{ref} to minimize the determination error to provide a sound initial trajectory for the second step. We utilized eight differently shaped torsos, among which we selected the one with a minor error.

We further optimized the electrode positioning and torso geometry to overcome deficiencies in imaging data. In the second step, we varied all dipolar locations $\mathbf{r}_k$ to minimize the error (5) using a gradient-based method (Gauss-Newton).

2.5. The heart model to represent EDTs

We constructed an appropriately oriented bi-ellipsoidal heart using cardiac MRI data with the left (LV) and right (RV) ventricles. The heart's long axis coincided with the LV axis, whereas the short axis perpendicular to the former pointed at the septum center.

Due to the uncertainty of realistic reference location in the absence of imaging data, we attached the reference location to the heart's mass center point obtained from cardiac MRI studies [9], assuming that the ED trajectory center coincides with the center of the bi-ventricular heart. This procedure helped to visualize EDTs in the heart's local coordinate system, enabling description in the LAO, RAO, and the four-chamber views (4C).

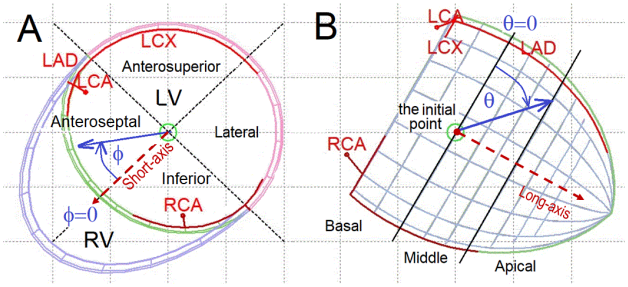

Figure 1. A: The LAO view with the wall segments. B: The RAO view with the wall regions. RCA, LCA, LAD, and LCX are the coronary arteries.

We used a 12-segment LV subdivision with four quadrants (1: anteroseptal, 2: anterosuperior, 3: lateral, 4: inferior), enumerated by roman numbers in Figure 2A, and three regions (1: apical, 2: middle, 3: basal) in Figure

2B [10]. We related quadrants (q) and regions (r) to the blood-supplying arteries: the left anterior descendent (LAD), left circumflex (LCX), and right coronary (RCA) artery. The myocardial segment number (MSN) was provided by

$$MSN = 3q + r. \quad (6)$$

We considered that LAD supplies segments 1-5 and 10, LCX 6 - 9, and RCA 11-12, respectively. For a more straightforward calculation, we modified the standardized definition of MSN [10], exchanging the quadrants 3 and 4 in (6).

The LAO view defined azimuth φ increasing during clockwise rotation, -180º ≤ φ ≤ 180º. The RAO view defined elevation ϑ with ϑ=0 in the equatorial plane and increasing from the basal to the apical orientation, -90º ≤ ϑ ≤ 90º. Azimuthal angle determined the quadrants and elevation angle of the regions. Specifically, the quadrants run from 1 to 4 when increasing azimuth φ by 80º, whereas the basal region was defined for ϑ≤ -25º, middle for -25º ≤ϑ≤ 45º and apical for ϑ>45º.

For localization of ventricular segments supplied by the occluded artery, we determined the intersection of the model ventricular wall with the ED vector at the ST segment end, which provided angles ϑ and φ in the heart's coordinate system and MSN according to (5).

2.6. ECG signal processing

All recordings were five-minute (or more) supine resting 12-lead ECGs (sampling rate of 1 kHz, 300 Hz low pass filter) providing nine signals (VR, VL, VF, V1…V6) necessary to assess EDTs. After identifying beats, we constructed a template signal using signal averaging from the five most similar beats and delineated the ECG waves. We used the STAFF III study protocol to isolate short ECG segments (20 s) from the recordings to create the baseline and occlusion specimen sets. The former was obtained from recordings before or after the vessel occlusion and the latter during three instants of the balloon inflation at 1, 3, and 5 min of occlusion, respectively. We used both sets to test the quality and reproducibility of the method.

Finally, the error Err=1-Rcc and the average RMS error between the reconstructed and the original ECG were computed as a measure of the quality of the method.

3. Results

We collected 741 ECG specimens, 360 and 384, from the baseline and occlusion sets, respectively. After the first optimization step that provided the best torso, the mean ± SD error of determination Err = ($1-R_{cc}$) was 2.1 ± 1.4 %, N=741. The non-selected torso shapes provided errors from up to twice more significant values to very close ones that often led to the selection of different torsos of similar shapes in different recordings of the same patient.

The values of the propagation parameters k_{QRS}, k_T, and tau for all 741 specimens were 44.8 ±15.3 cm/s, 7.7 ±1.5 cm/s, and 45.3±1.5 ms, being significantly bigger only in k_T ($p<10^{-4}$).

After the second optimization, Err fell to 0.83 ± 0.06 %, i.e., more than twice, and the RMS error was 5.5 ±1.3 μV. Err was significantly higher in the occlusion than in the baseline set, 0.9 ± 0.6 % vs. 0.77± 0.5%, p=0.002. To support the hypothesis of ED propagation along its vector direction, we compared the instantaneous ED trajectory and dipole directions by calculating their average mutual angle (α) over the EDT course. The median α was 6° with 5 and 95 percentiles of 1° and 31°, respectively.

3.1. The EDT behavior during occlusion

Immediately after the balloon inflation causing the artery occlusion, the EDT shape transformed dramatically by leaving its typical depolarization path well before the QRS end. It either swapped toward the culprit artery segment (usually LDA) or proceeded the mid-QRS EDT course (usually RCA and LCX), extending its course during the ST segment and early T wave towards the myocardial segment of the culprit artery (Fig. 2).

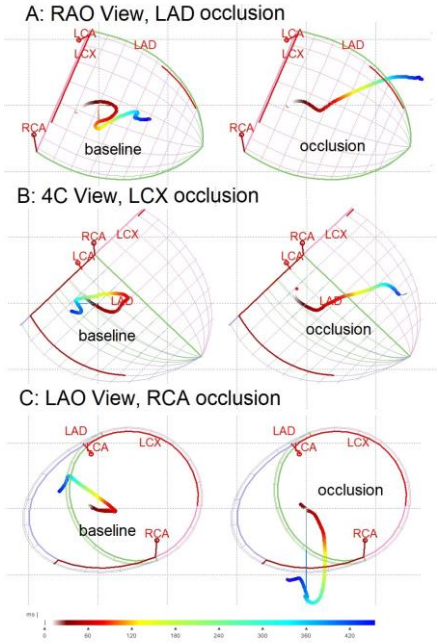

Figure 2. The EDT dynamics before and during occlusion of the coronary arteries. We used the view with the most significant response. Left, baseline; Right, occlusion. The color coding is adopted from [1].

Considering 384 ECG specimens from the occlusion set, we found that the localization of the corresponding myocardial segments was reasonable in LAD (in 92% of 145 specimens) and LCX (in 78% of 88 specimens) and

deficient in RCA (in 45% of 146 specimens) (Table I, Figure 3).

Table I. Frequency distribution of the model-derived myocardial segments concerning the occluded artery

Artery/MSN	N_{tot}	1-3	4,5	6-9	10	11,12
RCA	145	*33*	0	36	*10*	**66**
LCX	88	3	1	**69**	4	11
LDA	144	**120**	**11**	0	**3**	*10*
LV main	9	6	3	0	0	0

MSN, myocardial segment number; N_{tot}, the total number of ECG specimens from the occluded artery; RCA, LCX, and LDA, LV main, the coronary arteries; Domicile and borderline regions are designated in bold and italic numbers, respectively;

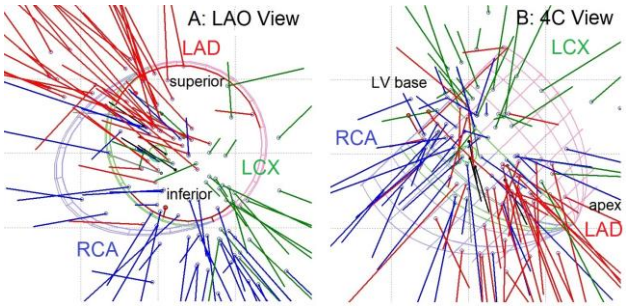

Figure 3. The distribution of the ST segment's EDs with their positions and orientations 3 min after the occlusion of the corresponding coronary artery. Panel A, the LAO view. Panel B, the four-chamber (4) view. RCA occlusion forces the ED's orientation mostly towards the inferior wall (A) and partially to the apex (B), that of LCX towards the inferior-posterior wall (A) and the right ventricle (B), and LDA occlusion towards the anterosuperior wall (A) and the apex. The overlapping of regions with different artery supplies is minor. Color coding: RCA, LCX, and LAD EDs are in blue, green, and red color, respectively.

4. Discussion and Conclusion

Using a novel space ECG method, we showed that the ED trajectories assessed from the 12-lead ECG using the BEM model consistently reproduce measured ECG signals reaching a precision below 10^{-2}. This view is consistent with Burger's concept of a complex lead vector [11] that, in our case, depends on the properties of the torso besides the geometrical ones (2).

We introduced the concept of variable propagation speed v_{ED} due to the need to find a good trajectory approximation to initiate the optimization. Though it succeeded in reducing the error of determination and shortened the calculation time, we do not know how it affected the optimization course.

We confirmed the hypothesis that during acute myocardial ischemia, the QRS end and ST segment's EDTs reveal the location of ischemia, which might aid its detection. Our results are consistent with the known distribution of myocardial segments affected by the corresponding culprit arteries in myocardial ischemia. Since the missed localizations belonged only to the neighboring segments, a more appropriate blood supply distribution area could be found by finely adjusting the segment borders.

References

[1] M.J. Boonstra, D.H. Brooks, P. Loh, and P.M. van Dam, "CineECG: A novel method to image the average activation sequence in the heart from the 12-lead ECG," Comput. Biol. Med., vol. 141, pp. 105128, Feb 2022.

[2] V. Starc, and T.T. Schlegel, "Moving dipole determination from 12-lead ECGs can improve detection of acute myocardial Ischemia," Computing Cardiol., vol. 47, pp.1-4, 2020.

[3] W. Bystricky, "Identification of strict left bundle branch block using a moving dipole model," Computing in Cardiol., vol. 45, p.1-4, 2018

[4] S.G. Warren, and G.S. Wagner, "The STAFF studies of the first 5 minutes of percutaneous coronary angioplasty balloon occlusion in man", *J Electrocardiol*, vol. 47, pp.402–407, 2014.

[5] V. Starc, "Equivalent dipole trajectories assessed from the 12-lead ECG using a tailored human torso model," Computing Cardiol., vol. 48, pp.1-4, 2021.

[6] T.F. Oostendorp and A. van Oosterom, "Source parameter estimation in inhomogeneous volume conductors of arbitrary shape ."IEEE Trans. Biomed. Eng., vol. 36, p.382-391, March 1989.

[7] A.J. Pullan, L.K. Cheng, R. MacLeod, D.H. Brooks, et al., "The Inverse Problem of Electrocardiography," In PW Macfarlane et al. (eds.), Comprehensive Electrocardiology, p. 299-344. Springer, London 2010

[8] Nelder JA, Mead R. A Simplex method for function minimization. Comput J (UK) 1965; 7: 308-313.

[9] F. Odille, S. Liu, P. van Dam, and J. Felblinger, "Statistical. variations of heart orientation in healthy adults," *Computing Cardiol.*, vol. 44, pp.1-4, 2017.

[10] RH Selvester et al., "Myocardial Infarction," In PW Macfarlane et al. (eds), *Comprehensive Electrocardiology*. Springer, London 2010.

[11] H. C. Burger, and J. B. van Milaan, Br. Heart J., vol. 10, pp. 229-33, 1948.

Address for correspondence:

Vito Starc, MD, PhD
Ljubljana University, Faculty of Medicine
Zaloska 4, SI 1000 Ljubljana, Slovenia
E-mail: vito.starc@mf.uni-lj.si.